Geochemistry Geophysics Geosystems G3
AN ELECTRONIC JOURNAL OF THE EARTH SCIENCES
Published by AGU and the Geochemical Society

Article
Volume 6, Number 10
8 October 2005
Q10003, doi:10.1029/2004GC000867
ISSN: 1525-2027

Massive Early Cretaceous volcanic activity in the Nauru Basin related to emplacement of the Ontong Java Plateau

Kimihiro Mochizuki
Earthquake Research Institute, University of Tokyo, 1-1-1, Yayoi, Bunkyo-ku, Tokyo 113-0032, Japan (kimi@eri.u-tokyo.ac.jp)

Millard F. Coffin
Ocean Research Institute, University of Tokyo, 1-15-1 Minamidai, Nakano-ku, Tokyo 164-8639, Japan

Olav Eldholm
Department of Earth Science, University of Bergen, Allegt. 41, Bergen N-5007, Norway

Asahiko Taira
Center for Deep Earth Exploration, Japan Agency for Marine-Earth Science and Technology, 3173-25 Showa-machi, Yokosuka, Kanagawa 237-0061, Japan

[1] The Mesozoic Nauru Basin in the western Pacific was created by seafloor spreading in Late Jurassic and Early Cretaceous time and was subsequently affected by Early Cretaceous flood volcanism approximately contemporaneous with emplacement of the nearby ~120 Ma Ontong Java Plateau (OJP). To investigate structure and stratigraphy of the basin, we completed a coincident multichannel seismic reflection (MCS) and refraction (sonobuoy) transect from the center of the Nauru Basin to the eastern flank of the OJP in 1998 aboard R/V *Hakuho Maru*. Along the transect we identify four segments of distinct crustal structure: C1, a thick igneous complex with no observable refractions; C2, basaltic sills and flows, C3, faulted sediment and rock near the flank of the OJP; and C4, the OJP. On data from seven sonobuoys we observe P-wave refraction arrivals with apparent velocities of ~6.0 km/s in each segment except C1. Sonobuoy data from segment C1 show no refractions, a common phenomenon in the northern Nauru Basin. We consider that the structure in segment C1 is most representative of typical Nauru Basin crust, and we estimate the volume of the thick igneous complex from discrepancies between actual seafloor depths and those predicted by an age-depth model, which commonly exceed 1000 m. We selected an appropriate model by comparing observed seafloor depths at drill holes in the Mesozoic Pigafetta and East Mariana basins where Cretaceous igneous complexes are thin or absent. From an empirical density-velocity relation, we calculated a basalt loading factor of 780 m/s for subsidence of the Late Jurassic-Early Cretaceous oceanic crust. We then applied the factor to estimate the thickness of the younger Early Cretaceous igneous complex, using previous seismic reflection (Charcot 2), drilling (DSDP Site 462), and wide-angle seismic data from DSDP Site 462 as controls. We estimate that the igneous complex is thickest, ~5500 m, in the center of the basin and that the total volume of the Early Cretaceous igneous complex is 3.3×10^6 km^3.

Components: 10,231 words, 12 figures, 3 tables.

Keywords: igneous complex; Naura Basin; oceanic crust; seismic survey.

Index Terms: 0930 Exploration Geophysics: Oceanic structures; 3025 Marine Geology and Geophysics: Marine seismics (0935, 7294); 7220 Seismology: Oceanic crust.

Received 26 October 2004; **Revised** 23 May 2005; **Accepted** 20 July 2005; **Published** 8 October 2005.

Mochizuki, K., M. F. Coffin, O. Eldholm, and A. Taira (2005), Massive Early Cretaceous volcanic activity in the Nauru Basin related to emplacement of the Ontong Java Plateau, *Geochem. Geophys. Geosyst.*, *6*, Q10003, doi:10.1029/2004GC000867.

1. Introduction

[2] Much of the Earth's interior heat is dissipated by the formation of oceanic crust by seafloor spreading along mid-ocean ridges. However, because of their size and relatively instantaneous emplacement, the formation of large igneous provinces (LIPs) had a large impact on the Earth's energy balance at certain times in the past, and their formation may instigate global environmental change [e.g., *Tarduno et al.*, 1991; *Coffin and Eldholm*, 1993]. Calculations of the Earth's ocean crustal budget shows a 50% to 75% increase in production by both seafloor spreading and LIP emplacement during Cretaceous time, abruptly beginning at 125 Ma and ceasing at 80 Ma [*Larson*, 1991]. The coincidence between the initiation and duration of this Cretaceous pulse of crustal production, and those of the interval of normal magnetic polarity led *Larson* [1991] to propose a "mid-Cretaceous superplume" that originated near the core/mantle boundary. The surface manifestations, i.e., LIPs, of the hypothesized superplume now sit on some of the Earth's oldest (Jurassic; ~165 Ma) ocean floor along the Pacific Ocean's western rim [e.g., *Renkin and Sclater*, 1988]. The most prominent feature is the world's largest igneous province, the Ontong Java Plateau (OJP) [*Coffin and Eldholm*, 1993]. The OJP is situated among Jurassic-Early Cretaceous ocean basins: the Pigafetta (PB), the East Mariana (EMB) and the Nauru (NB) basins from north to south (Figure 1).

[3] These old and therefore deep ocean basins have been the focus of seismic surveys [*Abrams et al.*, 1993; *Shipley et al.*, 1993] and multidisciplinary analyses of igneous rock samples, primarily obtained by the Deep Sea Drilling Program (DSDP) and the Ocean Drilling Program (ODP) [e.g., *Castillo et al.*, 1991, 1994; *Castillo*, 2004; *Tejada et al.*, 2004], which have revealed Cretaceous volcanic activity in the form of basaltic sills and flows, and volcaniclastic sediments. In fact, among four drill sites in the three Jurassic-Early Cretaceous ocean basins, oceanic crust (Jurassic) was recovered from only one site in the PB (ODP Site 801) at 462 m below seafloor (mbsf), and the other three sites (PB ODP Site 800, EMB ODP Site 802, and NB DSDP Site 462) penetrated only Cretaceous sills and flows postdating the oceanic crust of the respective basins (Figures 1 and 2). In the PB and EMB, the top of these Jurassic or Cretaceous igneous rocks defines acoustic basement on seismic reflection data, which lies ~500 mbsf. The Jurassic oceanic crust is suggested from the seismic reflection stratigraphy tied to that at Site 801 to exist just underneath the basement [*Abrams et al.*, 1993].

[4] Of the Jurassic-Early Cretaceous basins adjacent to the OJP, morphologically the NB is most directly linked to the OJP because no structural boundary demarcates the two structures (Figures 1 and 3). Unlike the other two basins, water depths in the NB are mostly shallower than 5,000 m. In fact, NB seafloor is ~1000 m shallower than its age predicts, which has been postulated to result from widespread Cretaceous volcanic activity including emplacement of the OJP [*Renkin and Sclater*, 1988; *Shipley et al.*, 1993]. Questions arising from previous studies include: what depth does the top of the Jurassic-Early Cretaceous oceanic crust lie, what is the extent of Cretaceous volcanic activity in the basin, and how was the OJP emplaced on preexisting oceanic crust.

[5] To address such outstanding structural and stratigraphic questions, we conducted a multichannel seismic reflection (MCS), refraction, gravity, and magnetics survey in 1998 aboard R/V *Hakuho Maru* of the University of Tokyo's Ocean Research Institute. A short (~45 km) profile (Line 201) lies in the southernmost NB, and a major (560 km) E-W transect (Line 401) runs from the center of the basin to the eastern flank of the OJP (Figures 1 and 3). Thirteen sonobuoys were deployed along Line 401 for wide-angle reflection-refraction surveys. Both lines intersect a preexisting N-S MCS transect of the NB, Charcot 2 [*Shipley et al.*, 1993]. DSDP Site 462 is located on Charcot 2, enabling *Shipley et al.* [1993] to correlate reflections with stratigraphy from the drill cores.

[6] Herein we present results of KH98-1 MCS/refraction studies. By tying our data to the Charcot 2 and hence DSDP Site 462 data, we are able to increase our knowledge of the 3D structure and stratigraphy of the NB. We consider and evaluate age-seafloor depth relationships at three ODP boreholes in the Jurassic PB and EMB where oceanic crust was reached. We determine the most appropriate age-seafloor depth model for the Jurassic ocean basins in the western Pacific and apply it to the NB. We attribute discrepancies between observed and predicted seafloor depths to the voluminous Cretaceous igneous complex, and we estimate its thickness along the Charcot 2 profile. We then estimate depth to the yet unsampled Jurassic-Early Cretaceous oceanic crust in the NB, and calculate the volume of the Cretaceous igneous

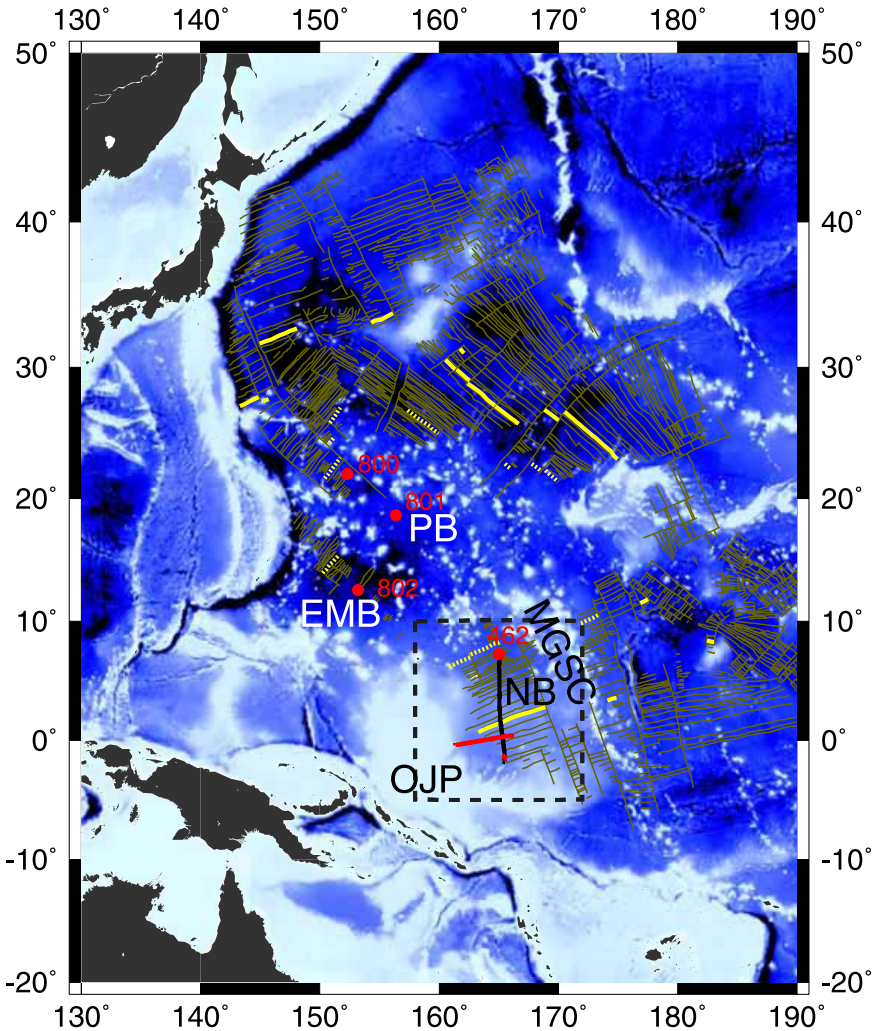

Figure 1. Topography map of the western Pacific. Dark yellow lines are magnetic anomaly lineations [*Nakanishi and Winterer*, 1998]. Thick light yellow lines indicate magnetic anomaly M19, which encompasses the Jurassic-Cretaceous boundary [*Gradstein et al.*, 1994]. Thick dotted light yellow lines depict M29 (~156 Ma), a part of which coincides with the northern boundary of the Nauru Basin. Thick red lines are 1998 R/V *Hakuho Maru* cruise KH98-1 MCS profiles. The north-south thick black line is the 1987 N/O *Charcot* Mesopac 1 MCS profile 2. Deep Sea Drilling Project (DSDP) and Ocean Drilling Program (ODP) drill sites 462, 800, 801, and 802 are shown by closed red filled circles. The dashed square indicates the area shown in Figure 3. EMB, East Mairana Basin; MGSC, Marshall-Gilbert Seamount Chain; NB, Nauru Basin; OJP, Ontong-Java Plateau; PB, Pigafetta Basin.

complex in the NB. Overall, we illuminate the development of the NB and OJP.

2. Background

[7] In this paper, we define the Nauru Basin in the western equatorial Pacific as a major oceanic deep encompassing 0.8 million km^2 (~1000 km NS × ~800 km EW) that is bounded to the north and east by the Marshall-Gilbert seamount chain, and to the west and southwest by the Ontong Java Plateau (OJP) (Figures 1 and 3), although some authors [e.g., *Shipley et al.*, 1993] may define the basin with a larger area. Late Jurassic (north) and Early Cretaceous (south) magnetic anomalies have been identified in the basin [*Larson*, 1976; *Cande et al.*, 1978; *Nakanishi et al.*, 1992; *Nakanishi and Winterer*, 1998] (Figure 3). Igneous rock samples have been recovered from the only drill site within the basin, DSDP Site 462 (Leg 61), that is located in the oldest and deepest part of the basin between magnetic anomalies M26 and M27 (~155 Ma). However, the two holes drilled at Site 462 did not reach Jurassic oceanic crust. The 1070 m section cored at Hole 462A consists of an upper 450 m of

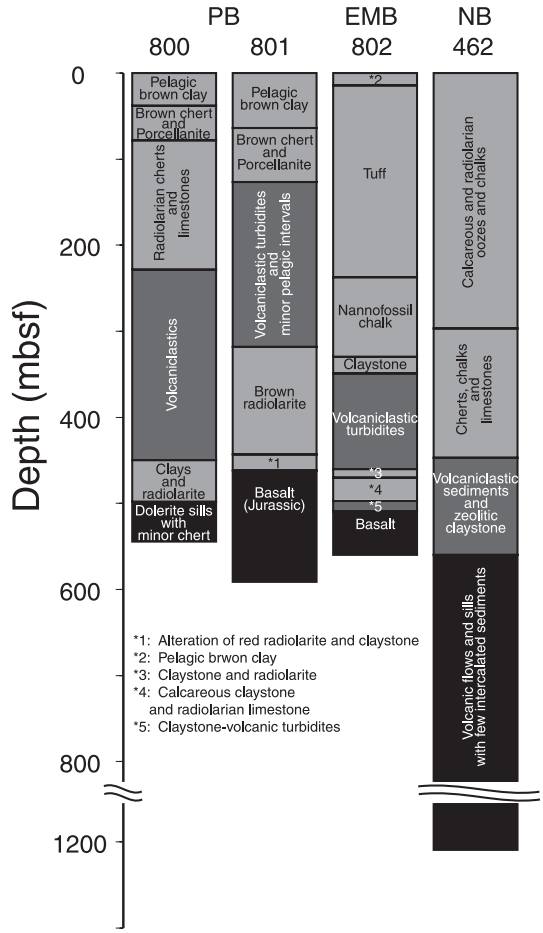

Figure 2. Lithology of drilled cores at ODP Leg 129 sites 800, 801, and 802 and DSDP Leg 61 Site 462. Jurassic oceanic crust was encountered only at Site 801, ~500 m below the seafloor (mbsf). In contrast, oceanic crust has not been penetrated in the NB, even after drilling ~1200 mbsf at Site 462.

sedimentary units, and a lower 500 m of igneous rock, with an intervening 113 m of volcaniclastic sediment (Figure 2). The igneous section was subdivided into an upper unit consisting of basalt sills with intercalated volcanogenic sediments, and a lower unit consisting of basalt sheet flows of variable thickness [*Larson and Schlanger*, 1981]. A $^{40}Ar/^{39}Ar$ age for the upper igneous unit is ~110 Ma (early Albian) [*Ozima et al.*, 1981]. Hole 462A was subsequently revisited during DSDP Leg 89, and an additional 140.5 m of core was obtained, making the total subseafloor penetration 1209 mbsf. However, Jurassic oceanic crust was not sampled, although minor pillow structures were identified [*Shipboard Scientific Party*, 1986]. The oldest age determined in Hole 462A was 129.7 Ma near the bottom of the hole [*Takigami et al.*, 1986]. Thus the >650 m thick igneous complex, overlain by 113 m of volcaniclastic sediment, suggests significant Early Cretaceous volcanic activity in and around the basin. The thicker Cretaceous igneous complex in the NB implies that, of the three Jurassic-Early Cretaceous basins, it was most affected by Cretaceous magmatism in the region. Geochemical results from the Cretaceous igneous rock in the NB and of OJP rock show similar general MORB-like compositions [*Castillo et al.*, 1991]. Therefore Cretaceous volcanic activity in the three ocean basins was likely related to emplacement of the adjacent OJP.

[8] The emplacement history of the OJP, however, remains enigmatic. Volcanic basement has been sampled from seven DSDP and ODP sites on the OJP, as well as from obducted OJP sections in the Solomon Islands, and it appears that most of the OJP formed at 122 Ma, with subsequent minor magmatism at 90 Ma [e.g., *Fitton and Godard*, 2004; *Tejada et al.*, 2004]. Several emplacement models have been proposed, including the mantle plume model [*Bercovici and Mahoney*, 1994; *Farnetani and Richards*, 1994] and the meteorite impact model [*Rogers*, 1982; *Ingle and Coffin*, 2004]. However, to date, no model explains all of the observations, such as chemical compositions of rock samples, magnetic anomaly patterns, hot spot locations, and vertical motion of seafloor, without case-specific assumptions [e.g., *Tejada et al.*, 2004].

[9] A key question in understanding the history of the NB is how Jurassic-Early Cretaceous magnetic anomalies were preserved during intense subsequent Early Cretaceous magmatism in the basin. Two explanations have been proposed. Basin-wide multiple sources of volcanism could have created basaltic sills and flows, allowing preservation of Jurassic-Early Cretaceous magnetic anomalies [*Shipley et al.*, 1993]. Alternatively, an Early Cretaceous seafloor spreading system in the northern NB developed following rifting of preexisting Jurassic oceanic crust, in which case current identifications of Jurassic-Early Cretaceous magnetic anomalies are erroneous [*Castillo et al.*, 1991]. The origin of the massive Early Cretaceous magmatism in the NB, as well as in the EMB and PB, has yet to be resolved [*Shipley et al.*, 1993].

[10] Interpreted depth to oceanic crust in the NB is more than 1000 m shallower than its Jurassic age predicts [*Renkin and Sclater*, 1988; *Shipley et al.*, 1993], even after correction for sediment loading [*Crough*, 1983]. *Nagihara et al.* [1996] ascribed the discrepancy between predicted and observed

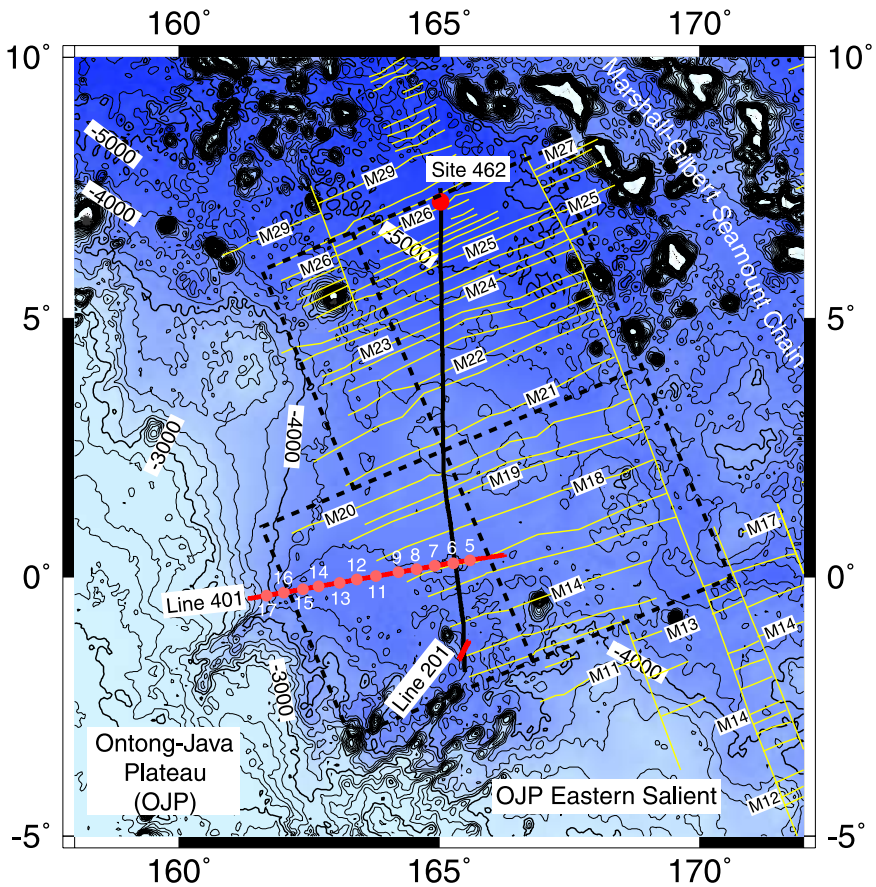

Figure 3. Tectonic setting of the Nauru Basin. Red lines and filled pink circles are 1998 R/V *Hakuho Maru* cruise KH98-1 MCS profiles and sonobuoy locations, respectively. DSDP Site 462 is indicated by a filled red circle near the northern end of the Charcot 2 profile. Mesozoic magnetic anomaly lineations are shown by yellow lines [*Nakanishi and Winterer*, 1998]. Bathymetric contour interval is 200 m. Dashed rectangles indicate partitioning for volume calculations of the igneous complex (see section 7).

seafloor depths to reheating of the old oceanic lithosphere. They found that relationships between heat flow values and observed seafloor depths of eight old ocean basins in the western North Pacific and the Atlantic are well explained by a simple boundary layer cooling model [*Parsons and Sclater*, 1977], and proposed that the NB experienced reheating that resulted in rejuvenation of its thermal age to be ~115 Ma. This thermal age seems to correlate well with Early Cretaceous magmatism represented by emplacement of the OJP at ~122 Ma.

[11] Seafloor depth anomaly and thick igneous complex at DSDP Site 462 suggests that widespread Early Cretaceous magmatism affected the NB; *Shipley et al.* [1993], for example, estimated the thickness of the Cretaceous igneous complex to be 1700 m from discrepancies between predicted and observed seafloor depths. *Gladczenko et al.* [1997] estimated by compiling existing refraction surveys [*Houtz*, 1976; *Wipperman et al.*, 1981] that the complex is 2150 m thick at DSDP Site 462. *Castillo* [2004] concluded that the 113 m of volcaniclastic sediment at Site 462 were derived from the OJP. Despite these studies, a comprehensive understanding of the origin and evolution of the NB has not yet been reached.

3. Data Acquisition and Processing

[12] MCS data were acquired using a 48-channel 1.2 km long solid hydrophone streamer along two profiles during R/V *Hakuho Maru* cruise KH98-1 in 1998: a 560 km long E-W transect from the center of the Nauru Basin to the eastern flank of OJP near the equator (Line 401), and a 45 km long SW-NE profile in the southernmost NB just north of OJP's eastern salient (Line 201) (Figure 3). Line 401 runs subparallel to magnetic anomaly M17, and therefore it samples structure of nearly the

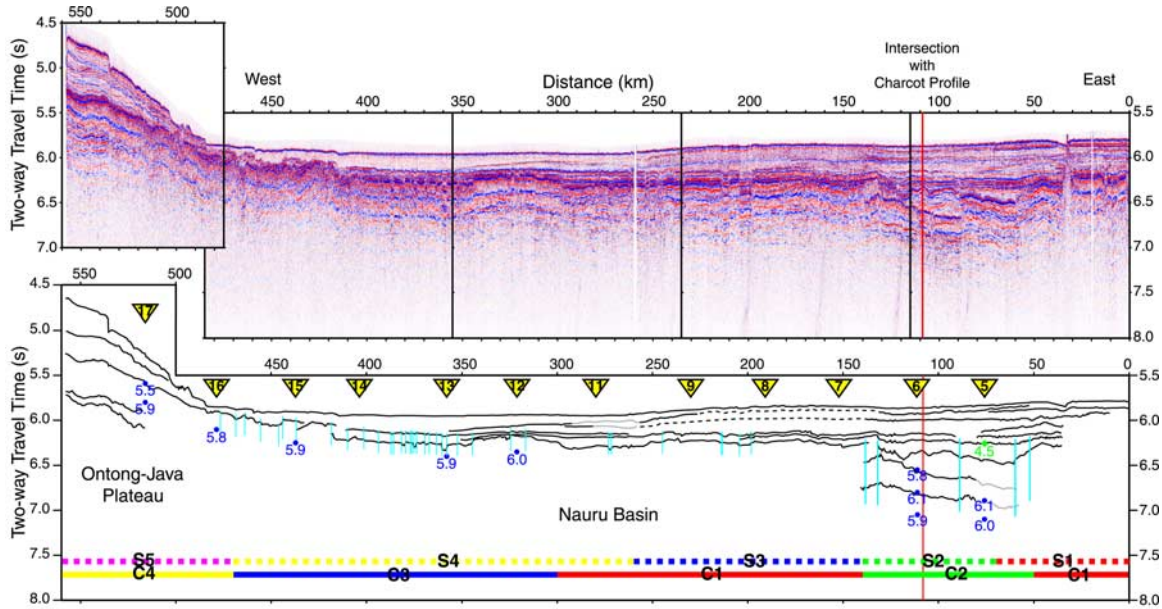

Figure 4. (top) The 1998 R/V *Hakuho Maru* cruise KH98-1 MCS profile 401 across the Nauru Basin and (bottom) interpretation of major reflection horizons. Gray lines indicate those picked with less confidence. Dotted horizons depict rough and disturbed horizons. Sonobuoy deployment locations are shown by inverted triangles (bottom). Locations of faults (light blue vertical lines) and interpreted sedimentary (S, dashed line) and crustal (C, solid line) structure segments are also shown. Blue dots indicate the top of refraction layers with P-wave velocities of ~6.0 km/s observed on data from respective sonobuoys, and a filled green diamond shows the top of a layer with a P-wave velocity of 4.5 km/s observed only on data from sonobuoy 5. Numbers accompanying those symbols indicate the observed velocities in km/s. Sonobuoys 5, 6, and 17 have refraction arrivals with ~6.0 km/s velocities from multiple layers (multiple filled blue circles for these sonobuoys). Red lines indicate intersection of Line 401 and the Charcot 2 profile. See Figure 3 for location of data.

same age (141 Ma) across the basin. Both lines 401 and 201 intersect the Charcot 2 profile [*Shipley et al.*, 1993] near the equator and at its southern end, respectively. Wide-angle reflection/refraction data were simultaneously collected using 13 sonobuoys deployed approximately every 40 km. Several different combinations of air guns were fired; a combination of two 20 l guns and one 17 l gun was used for most of the eastern half of Line 401, and a combination of one 20 l gun and one 17 l gun was used for most of the western half. To suppress coherent noise reverberating among layers, the firing of each shot was randomly shifted ±500 ms about the regular 20 s interval. The ship speed over the ground averaged 7 knots; therefore the spatial shot interval was ~72 m.

3.1. MCS Data

[13] Conventional processing techniques were applied to the MCS data. Predictive deconvolution was first applied to each shot gather both to attenuate air gun bubble oscillations and to suppress seafloor multiples. Spiking deconvolution was then applied to improve temporal resolution. After deconvolution, the MCS data were sorted into common midpoint (CMP) gathers with a 25 m CMP interval. Following velocity analyses, a frequency-wave number (F-K) filter was applied to further attenuate seafloor multiples. The traces were then stacked, and the CMP traces were processed with F-K migration, which was followed by frequency-distance (F-X) residual migration.

3.2. Sonobuoy Data

[14] Thirteen sonobuoys (5–17) were deployed along Line 401 (Figure 3). An additional sonobuoy (18) was deployed along a line running parallel to Line 401 a few hundred meters away when the vessel headed in the opposite direction. The sound velocity at the sea surface (1.54 km/s) was determined by observing travel times of the direct water wave assuming that drift speeds (2.08 kts to the west) of these sonobuoys (17 along Line 401 and 18 along Line 402) along the west flowing Equatorial Countercurrent were the same. Sound velocity in seawater is a function of salinity, temperature,

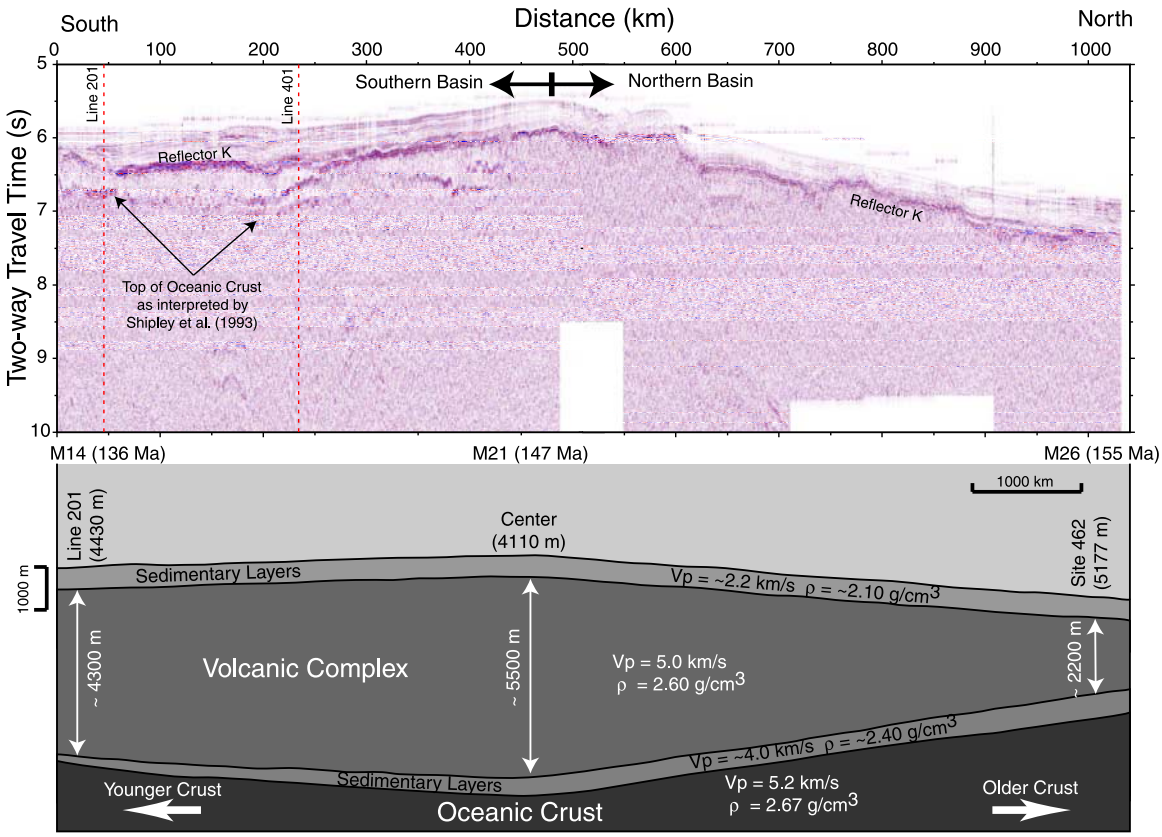

Figure 5. (top) The entire Charcot 2 MCS profile and (bottom) its interpretation (see Figure 2 for location). Sediment thickness varies from 0.3 to 0.5 s TWT. The seafloor is shallowest in the center of the basin, where its age is 147 Ma (magnetic lineation anomaly M21). The basin is divided into northern and southern basins near its center on the basis of reflection character: Prominent reflections from basaltic sills and flows are apparent in the southern basin but are absent in the northern basin. Thickness of the Cretaceous igneous complex is estimated from the difference between observed and estimated seafloor depths (see text and Table 2). Thickness of expected sedimentary layers between the bottom of Cretaceous complex and the top of oceanic crust may change according to the age of the crust; thicker sediment likely accumulated in the older northern part of the basin prior to the relatively instantaneous eruption of Cretaceous volcanic rock throughout the basin.

and pressure. Therefore we considered sound velocity at the sea surface to be constant for an east-west profile near the equator. Offsets between the sonobuoys and air gun shots were determined by observed travel times and the velocity of 1.54 km/s. We designed a band-pass filter of 5–20 Hz for the sonobuoy data to enhance refraction arrivals on the record sections.

[15] To derive a 1-D representation of velocity structure beneath each sonobuoy, we applied tau-p mapping to all of the sonobuoy data with applications of various techniques for noise suppression. However, none of the trials resulted in significant improvements. We estimated velocities and depths of refraction interfaces in two way travel time (TWT) by determining slopes of arrivals on the record sections and intercept times of reflection curvature, to which the arrival slope is tangent. Errors in calculated velocities and two way travel times are approximately 0.1 km/s and 0.05 s, respectively.

4. Results

4.1. MCS

4.1.1. Line 401

[16] The MCS data clearly image the structure and stratigraphy of the uppermost 1.5 s (TWT) of the NB from the basin's center to the eastern flank of OJP (Figure 4). The profile intersects the N-S trending Charcot 2 profile [*Shipley et al.*, 1993] (Figures 3 and 5). *Shipley et al.* [1993] interpreted the ages of prominent reflections on the Charcot 2 MCS data by stratigraphic correlation to DSDP Site 462. In turn, we tied the stratigraphy along Line 401

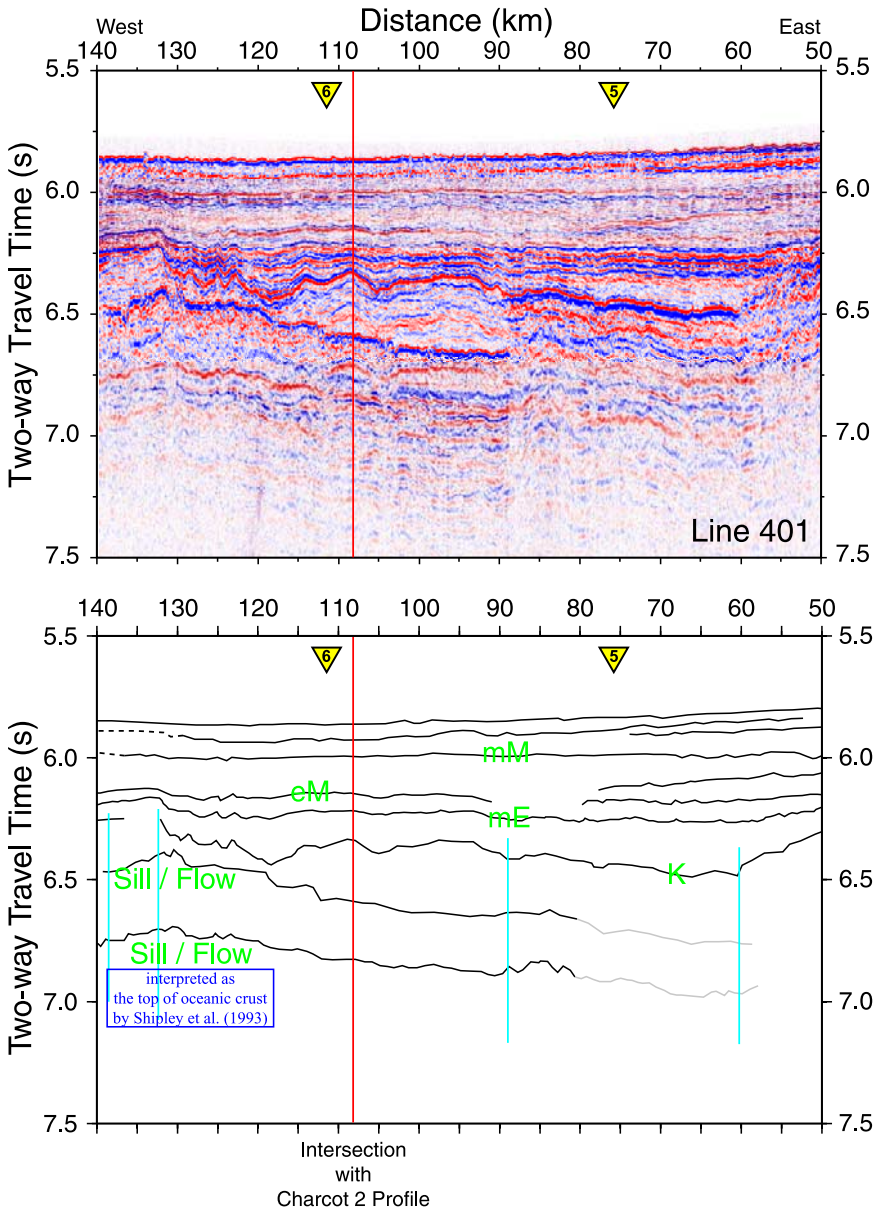

Figure 6. (top) Line 401 MCS data and (bottom) interpretation of major reflections and ages (mM, middle Miocene; eM, early Miocene; mE, middle Eocene; K, Cretaceous) in crustal segment C2 in the vicinity of the intersection with the Charcot 2 profile (see Figure 3 for location). Legends of horizons and faults are the same as Figure 4. Locations of sonobuoy deployments are shown as inverted yellow triangles. We correlate the tops of the seismic sequences at the intersection between Line 401 and the Charcot 2 profile according to the interpretations of *Shipley et al.* [1993], except for the deepest reflecting horizons. The deepest reflection was interpreted originally as the top of the oceanic crust [*Shipley et al.*, 1993]; we interpret the same reflection as the top of a sill or flow (see text).

to the Charcot 2 interpretations (Figure 6). A distinctive reflection marking acoustic basement through much of the basin correlates with the top of Lower Cretaceous volcanics (K in Figures 5 and 6). Sediment thickness thins from ~0.5 s TWT at the center of the basin to <0.1 s at the base of OJP. The reflection character of the sediment varies along the profile, along which we distinguish five major segments (Figure 4). Detailed stratigraphic interpretation of the sediment is not the focus of this study; hence we only summarize the segments briefly below, starting from the center of the basin:

[17] S1 (0 ~ 70 km): high amplitude, flat, continuous reflections.

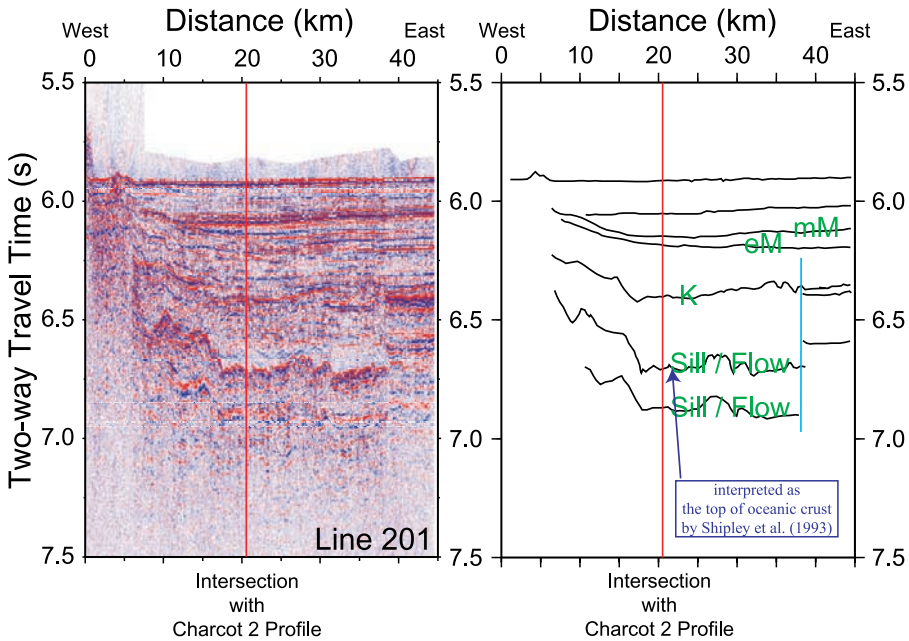

Figure 7. (left) Line 201 MCS data and (right) interpretation in the vicinity of the intersection with the Charcot 2 profile (see Figure 3 for location). We correlate the tops of the seismic sequences at the intersection between Line 201 and the Charcot 2 profile according to the interpretations of *Shipley et al.* [1993], except for the deepest two reflecting horizons. We interpret the interface indicated by a blue arrow as a sill/flow (see text), whereas *Shipley et al.* [1993] interpreted it as the top of oceanic crust. A prominent structural discontinuity is located at 35 km. All reflections ascend to the west, where a seamount lies beyond the profile.

[18] S2 (70 ~ 140 km): continuous reflections, slightly disturbed in the uppermost layers. Amplitudes are weaker than those in Segment S1.

[19] S3 (140 ~ 260 km): diffuse, discontinuous reflections. A gentle mound crests near the center of the segment. The segment may represent the path of one or more debris flows.

[20] S4 (260 ~ 470): reflection-free sequence overlying a basal sediment layer contiguous from S3 that onlaps acoustic basement at 360 km. The overall thickness of the sedimentary section does not change substantially.

[21] S5 (470 ~ OJP): probable hemipelagic sediment with increasing thickness toward the main OJP, especially above the carbonate compensation depth of 4,000 m (~5.3 s TWT).

[22] Although the profile runs subparallel to magnetic anomaly M17, thereby imaging structure of corresponding age (141 Ma), we observe distinct structural characteristics along the transect (Figures 4 and 6). Several prominent vertical faults (~50, 90, and 140 km) disrupt the center of the NB. The faults at ~50 and 140 km sandwich deeper reflections dipping to the SE (130°) at angles of ~0.86° at the intersection with the Charcot 2 profile (Figure 6). *Shipley et al.* [1993] interpreted these reflections as sills and flows by their reflection characteristics. Approaching the transition between the NB and the OJP, several faults disrupt continuity of reflections. At the transition, acoustic basement forms a rough, high relief horizon. On the basis of our interpretations, we classify the uppermost igneous (likely containing interbedded sediment) section along the transect into four major segments:

[23] C1 (0 ~ 50; 140 ~ 300 km): thick volcanic complex that dominates the basin.

[24] C2 (50 ~ 140 km): traces of sills and flows at varying depths (Figure 5).

[25] C3 (300 ~ 475 km): densely faulted section at the NB-OJP transition; acoustic basement shows high relief.

[26] C4 (~475 km): the OJP.

[27] Deep structure along the entire profile is not well resolved in the MCS data with the exception of sills and flows in C2 (Figure 6), where the Charcot 2 profile intersects Line 401 (Figures 3, 4, 5, and 6). As addressed in section 7, deep and rather ambiguous reflections observed below the

Table 1. Observed Refraction Arrivals and Estimated Depths in Two Way Travel Time to the Tops of Refraction Layers[a]

	P1		P2		P3		S	
Sonobuoy	P Vel, km/s	Intercept, s TWT	P Vel, km/s	Intercept, s TWT	P Vel, km/s	Intercept, s TWT	S Vel, km/s	Vp/Vs
5	4.53	6.44	6.11	6.89	6.05	7.1	–	–
6	5.83	6.55	6.08	6.8	5.93	7.05	3	1.93
7	–	–	–	–	–	–	–	–
8	–	–	–	–	–	–	–	–
9	–	–	–	–	–	–	–	–
10				NO CARRIER SIGNALS				
11	–	–	–	–	–	–	–	–
12	6.06	6.35	–	–	–	–	2.9	2.1
13	5.9	6.4	–	–	–	–	–	–
14	–	–	–	–	–	–	–	–
15	5.91	6.25	–	–	–	–	3.1	1.8
16	5.77	6.1	–	–	–	–	3	2
17	5.52	5.59	5.88	5.8	–	–	3	1.93

[a] A dash indicates that no refraction arrivals were observed.

top of interpreted volcanic rock along the profile, except within C2, do not coincide with any refraction/reflection interfaces observed in the sonobuoy data. They are considered to be either source bubble oscillations or internal multiples that have not been removed by deconvolution. In contrast, deeper reflections in C2 originate from distinct interfaces of sills and flows that give rise to refraction arrivals, with Vp of ~6.0 km/s, on the sonobuoy data.

4.1.2. Line 201

[28] In this short line in the southern NB, just north of the OJP's eastern salient (Figure 3), flat, layered sediments are underlain by reflections with high relief between 6.5 and 7.0 s TWT (Figure 7). Stratigraphy was tied to Charcot 2 interpretations. We observe a discontinuity at 35 km. Reflections ascend to the southwest, where a seamount lies beyond the end of the profile. The next-to-deepest reflection has been interpreted previously as the top of oceanic crust [*Shipley et al.*, 1993].

4.2. Sonobuoys

[29] Data from seven sonobuoys show refracted arrivals (Table 1), albeit of low amplitude slightly over the detection level, which is common for sonobuoy data in the region [*Wipperman et al.*, 1981; *Shipley et al.*, 1993]. Sonobuoys deployed over crustal segment C1 (Sonobuoys 7–11) do not show any refracted arrivals. Two adjacent sonobuoys (6 and 7) separated by only ~40 km highlight differences in refraction data (Figure 8); 6 recorded refraction arrivals with apparent velocities of ~6.0 km/s, whereas no refraction arrivals were recorded by 7.

[30] Analyses of all seven sonobuoys recording refractions yield apparent velocities of ~6.0 km/s (Table 1). Two sonobuoys recorded refractions with slower apparent velocities: 5 deployed over C2, characterized by distinctive basaltic sills and flows, and 17 over the OJP. Sonobuoy 5 recorded arrivals with an apparent velocity of ~4.5 km/s originating from an interface interpreted as the top of a chert-limestone layer (mE) by *Shipley et al.* [1993] (Figures 4 and 6). The interface where arrivals with an apparent velocity of ~5.5 km/s originate on 17 coincides with acoustic basement of the OJP. Why refracted arrivals with slower velocities are absent on most of the sonobuoy data is attributed to insufficiently thick sediment sections except in C2 and C4. We observe converted S-wave arrivals on three of the seven sonobuoys recording refracted P-wave arrivals. These arrivals have apparent velocities of ~3.0 km/s, which results in a Vp/Vs ratio of ~2.0.

[31] Multiple refraction arrivals were recorded by sonobuoys 5 and 6 in C2. The refraction interfaces of those arrivals coincide with the top of basaltic sills and flows observed on MCS data (Figure 4). Data from 6 show a relatively good signal-to-noise ratio (Figure 8), allowing identification of several refractions from interfaces at different depths. Arrivals on the two sonobuoys originate from basaltic sills and flows at different

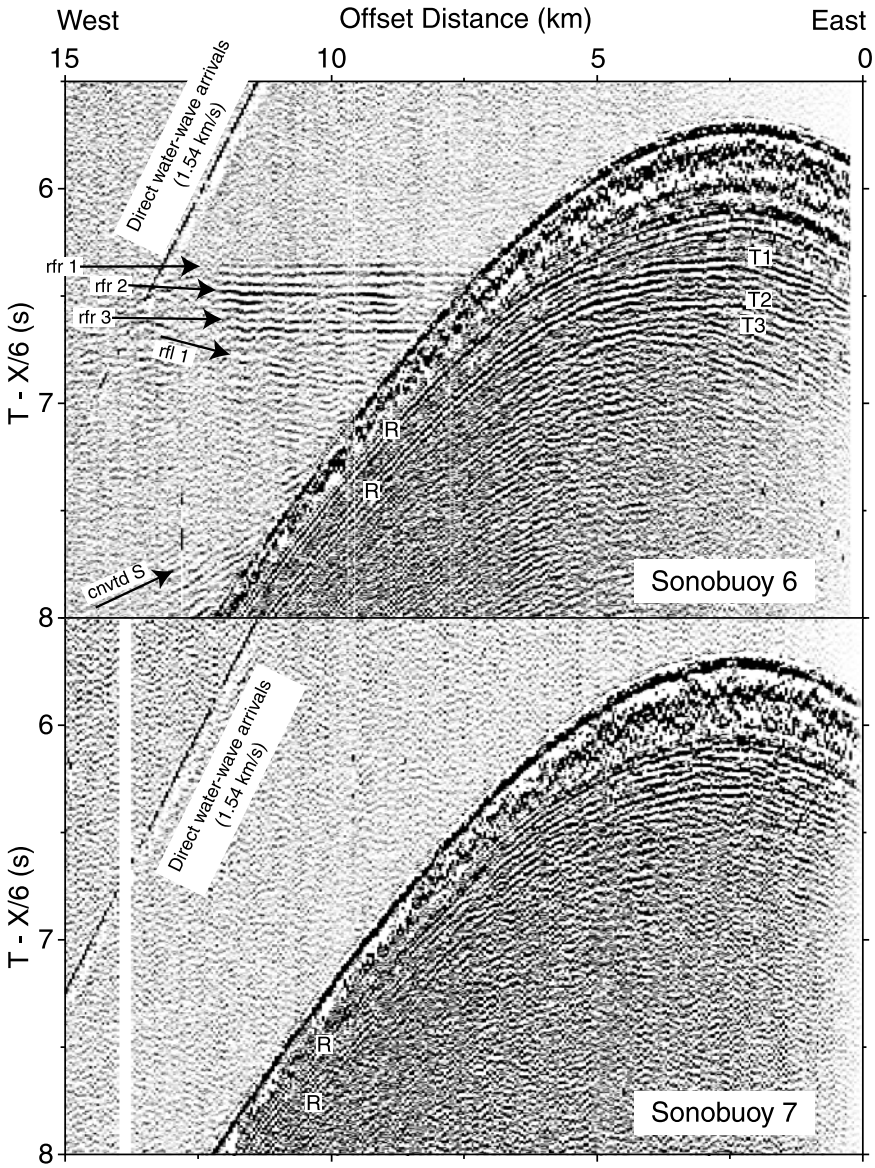

Figure 8. (top) Sonobuoy 6 and (bottom) 7 data plotted with a reduction velocity of 6.0 km/s. A 5–20 Hz band-pass filter was applied. Three series of weak refraction arrivals with slightly different P-wave apparent velocities of ~6.0 km/s are observed on sonobuoy 6, but not on sonobuoy 7, despite only ~40 km between the two data sets (see Figure 3 for location). We also recognize weak reflection arrivals after the refraction arrivals on sonobuoy 6 data, although identification of their onsets and phase correlations is difficult. The intercept time of such reflection arrivals may be ~7.7 s TWT. Arrivals of converted S-wave can also be seen on sonobuoy 6 data. Direct water wave arrivals can be recognized to ranges of ~15 km, to which source-receiver offsets are well controlled. Reflections to which the refraction arrivals are tangent are labeled with "T" on the sonobuoy 6 record. Those arrivals considered to be internal multiples within the curvature of the seafloor reflections are labeled with "R."

depths, and their apparent velocities range from 5.8 ~ 6.1 km/s (Table 1, Figure 4). Reflection arrivals from deeper structure can also be recognized on the 6 data (Figure 8), although the signal-to-noise ratio for these arrivals does not permit identification of their onsets. The deepest interface indicated by refraction arrivals in C2 is not observed on the reflection section (Figures 4 and 6).

[32] In C3 and C4 from the NB to the OJP (Figure 4), we observe refraction arrivals from a contiguous single interface with apparent velocities of ~6.0 km/s. This interface lies below the

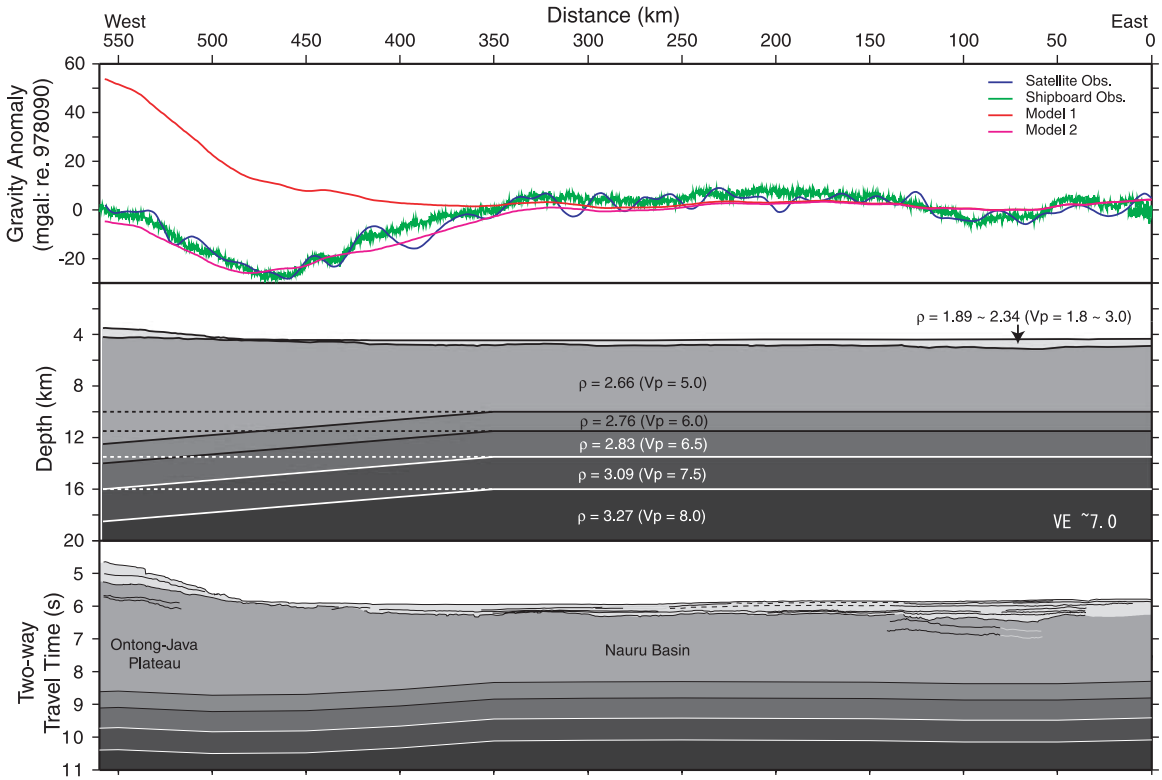

Figure 9. (bottom) Interpretation of major reflection horizons, (middle) structure, and (top) corresponding shipboard (green), satellite (blue), and modeled (red and pink) gravity data for Line 401 (see Figure 3 for location). Gravity anomalies are calculated for two models: Model 1 is horizontally homogeneous below the interpreted volcanic rock, and Model 2 includes flexure of the oceanic crust resulting from emplacement of the OJP onto preexisting Nauru Basin. The middle figure shows the structure of Model 2 (solid lines). Dashed lines beyond 350 km depict layer interfaces of the horizontally homogeneous Model 1. See text for gravity modeling parameters. Because structure within the Nauru Basin should be horizontally homogeneous, at least along the profile subparallel to the magnetic anomalies and hence isochrons, we normalized the calculated values to the observed values in the Nauru Basin. The calculated gravity profile for Model 1 correlates well in the Nauru Basin but diverges approaching the flank of the OJP at ~350 km. The shape of observed gravity at the OJP's flank suggests the existence of flexure of the underlying oceanic crust resulting from loading by the OJP. Gravity anomalies were also estimated for Model 2 incorporating flexure. Although Model 2 is not a unique solution, it fits the observations well. Vertical exaggeration of depth section (middle) is ~7.

deepest reflection recognized on MCS data that forms acoustic basement (Figure 4), which implies deeper structure than that resolved in the MCS sections.

5. Gravity

[33] Shipboard gravity data were acquired coincident with the MCS and wide-angle profiles. To examine basin structure, we undertook 2-D gravity modeling following estimation of NB and OJP densities and velocities [*Talwani et al.*, 1959]. Two models were constructed (Figure 9). The first model represents a simple horizontally layering structure below the acoustic basement across the NB to OJP. We assumed that P-wave velocities (Vp) within the sedimentary layers increase linearly from 1.8 to 3.0 km/s with depth. The sedimentary layer is underlain by the igneous complex. Although the sonobuoys recorded refraction arrivals with Vp as high as ~6 km/s, it is assumed that the average velocity of the igneous complex is ~5 km/s by referring to a velocity structure obtained at DSDP Site 462 [*Gladczenko et al.*, 1997]. We estimate its thickness from an age-seafloor depth relationship, as described in the next section. Below the Cretaceous igneous complex lies horizontally layered oceanic crust with a velocity structure taken from *Gladczenko et al.* [1997]. The second model includes flexure of the underlying oceanic crust due to the emplacement of OJP. The flexure is

Table 2. Nauru Basin Observed and Predicted Seafloor Depths Corrected for Sediment Loading, and Estimated Thickness of the Cretaceous Igneous Complex[a]

	Site 462	Center	Line 401	South End (Line 201)
Age, Ma	155 (M26)	147 (M21)	141 (M17) ~ 144 (M18)	136 (M14)
Observed depth, m	5177	4110	4350 ~ 4460	4430
Corrected depth, m	5417	4350	4590 ~ 4700	4670
BL, m (difference)	6857	6744	6656 ~ 6700	6582
	(1440)	(2394)	(2066 ~ 2000)	(1912)
PS, m (difference)	6129	6092	6061 ~ 6077	6033
	(712)	(1742)	(1471 ~ 1377)	(1363)
GDH1, m (difference)	5618	5609	5602 ~ 5606	5595
	(201)	(1259)	(1012 ~ 906)	(925)
Estimated thickness of igneous	2230	5464	4631 ~ 4337	4288
complex in meters and second TWT	0.91	2.23	1.89 ~ 1.77	1.75

[a] Ages of magnetic anomalies from *Gradstein et al.* [1994].

introduced below C3 of the reflection profile at the NB-OJP transition. We estimated densities of these structure models according to a Vp-density relationship [*Hamilton*, 1978]. The 2-D forward modeling method by *Talwani et al.* [1959] gives a relative gravity profile of a respective crustal section, and the resulted anomalies may be accordingly shifted. We consider the structure of the NB to be relatively homogeneous along the profile that is subparallel to the magnetic lineations, so the gravity anomaly is small in the basin. Therefore we normalized the calculated gravity profiles to the observed gravity values in the NB. The calculated gravity profile for the first model diverges from the observation at 350 km approaching the OJP (Figure 9). In contrast, the calculated profile for the second model agrees with the observations quite well. Although the second model may not be the only solution that explains the observed gravity profiles, introducing flexure of the underlying oceanic crust provides a simple and reasonable explanation of the observations.

6. Age-Depth Relationships

[34] Magnetic lineations in the NB trend ENE and young toward the south (Figure 3) [*Larson*, 1976; *Cande et al.*, 1978; *Nakanishi et al.*, 1992; *Nakanishi and Winterer*, 1998]. The northern end of the basin is bounded by anomaly M29 (~157 Ma, or Late Jurassic), and the southern end by anomaly M14 (~136 Ma, or Early Cretaceous), indicating that the NB north of the OJP's eastern salient formed in ~24 m.y. According to a plate model (PS [*Parsons and Sclater*, 1977]), depth to seafloor in the NB is shallower than predicted for its age [*Renkin and Sclater*, 1988]. The same holds true for a boundary layer model (BL [*Parsons and Sclater*, 1977]), and a different plate model (GDH1 [*Stein and Stein*, 1992]). Sediment loading depresses the oceanic crust to greater depths than it would be without sediment. *Crough* [1983] determined a correction factor for sediment loading of 600 m/s from sediment density and velocity profiles obtained from drill holes; corrected depths may be calculated by multiplying the factor by a sediment thickness measured in seconds of TWT. We applied the correction factor for observed sediment thicknesses (in s TWT), ranging from 0.3 to 0.5 s [*Shipley et al.*, 1993] before comparing observed and predicted seafloor depths (Table 2). We used a constant correction value of 240 m, corresponding to a sediment thickness of 0.4 s, which introduces an error of ±60 m (0.1 s TWT variations in thickness). The GDH1 plate model was tuned to fit older seafloor, so it predicts depths better than PS, but only slightly (Figure 10). The predicted BL depths range from 1440 to 2393 m deeper than the observed depths corrected for sediment loading. Respective differences for the PS model are 712 to 1742 m, and for the GDH1 model, 201 to 1259 m. Differences are greatest in the center of the basin, where the seafloor depth is the shallowest.

[35] We analyzed ODP drill holes in the PB and EMB, where one (Site 801) of the three holes reaches true Jurassic oceanic crust, similarly. Therefore evaluation of the three models (PS, BL, and GDH1) is possible. Lower Cretaceous basalts were sampled from acoustic basement at the other two drill sites, 800 and 802. However, the thickness of the Cretaceous igneous complex is probably thin, as inferred from the reverberant reflection

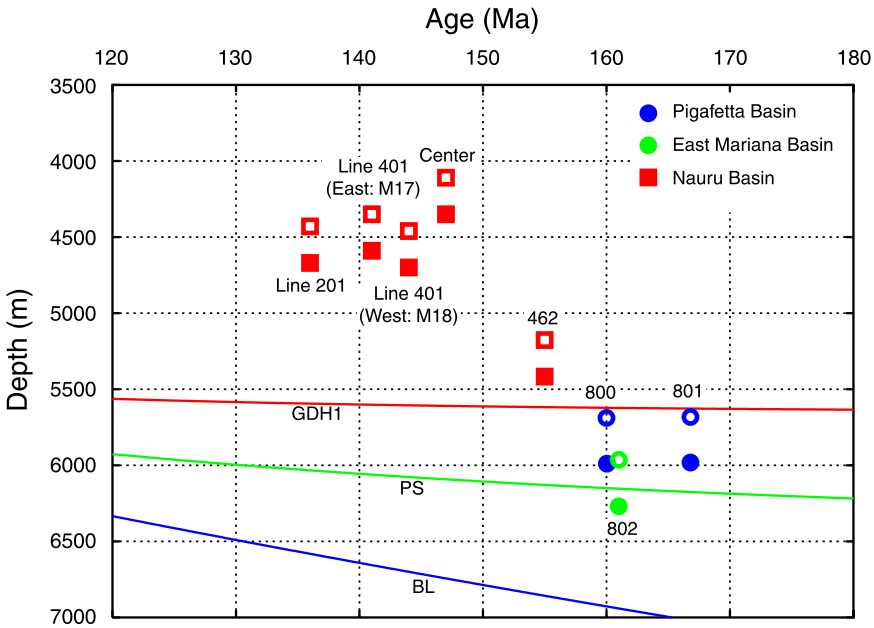

Figure 10. Age-seafloor depth plots from four DSDP and ODP drill sites in the three Jurassic-Early Cretaceous basins of the western Pacific, from the Charcot 2 profile in the center of the Nauru Basin, and from intersections with KH98-1 MCS profiles 201 and 401 (see Figure 3 for location). Open and filled symbols depict observed and corrected (for sediment loading) seafloor depths, respectively (Tables 2 and 3). Also shown are age-seafloor (corrected) depth curves estimated by three models: boundary layer (BL) and plate (PS) models of *Parsons and Sclater* [1977] and the plate model (GDH1) of *Stein and Stein* [1998].

character of acoustic basement. Such a reverberant character is absent in reflection data around Site 801, presumably due to a corresponding absence of a Cretaceous igneous complex overlying Jurassic oceanic crust [*Abrams et al.*, 1993]. On the basis of seismic reflection data, we assigned a constant sediment thickness of 0.5 s TWT at these holes. The $^{40}Ar/^{39}Ar$ age determined for samples of Jurassic oceanic crust from Site 801 is 166.8 Ma, and the ages at the other two sites were estimated from extrapolation/interpolation of magnetic lineations in the basins [*Abrams et al.*, 1993]. For these two basins, PS estimates seafloor depths better than GDH1; differences between predicted and observed depths are <200 m for the former, but as much as 641 m for the latter (Table 3). Therefore we consider that PS is more suitable for predicting seafloor depths in the EMB and PB corrected for sediment loading.

[36] When PS is employed for estimating the seafloor depth in the NB, however, the discrepancy between observed and predicted depths is 1742 m in the center of the basin. This discrepancy may be attributed to additional loading of the Cretaceous igneous complex onto preexisting Jurassic oceanic crust. In the next section, we examine the expected depth of Jurassic oceanic crust through application of the above hypothesis.

7. Discussion

[37] Sonobuoys deployed over C1 show no refraction arrivals, a common characteristic of the northern NB [*Shipley et al.*, 1993]. We speculate that C1 and the northern NB share an igneous complex with relatively constant velocities. Therefore the seismic structure along the Charcot 2 profile in the southern NB may be anomalous compared to the more typical structure of the NB igneous complex. The anomalous structure may be limited to the ~90 km width of C2 in the southern NB (Figures 4 and 5).

[38] Several reflection curvatures are prominent on sonobuoy 6 and 7 data following seafloor reflection arrivals (R in Figure 8). Those arrivals remain within and converge toward seafloor reflection arrivals on both sonobuoy records, and maintain a characteristic ringing signature at a constant interval of ~0.17 s. Therefore we consider those arrivals to be internal multiples, or reverberant reflections. Although processing should suppress such arrivals on the MCS data,

Table 3. Pigafetta and East Mariana Basin Observed and Predicted Seafloor Depths, Corrected for Sediment Loading, at Drill Sites[a]

	Site 800	Site 801	Site 802
Age, Ma	160	166.8	161
Correction amount	300	300	300
Observed depth, m	5686	5682	5964
Corrected depth, m	5986	5982	6264
BL, m (difference)	6927	7020	6941
	(941)	(1038)	(677)
PS, m (difference)	6150	6175	6154
	(164)	(193)	(−110)
GDH1, m (difference)	5622	5627	5623
	(−364)	(−355)	(−641)

[a] Ages of magnetic anomalies from *Gradstein et al.* [1994].

they have not been completely removed, and we attribute at least some reflections below the top of interpreted volcanic rock (>∼6.3 s TWT) (Figure 4) to reverberant energy. However, other reflection arrivals within the curvature of the seafloor reflections in the sonobuoy 6 data clearly show higher intercept velocities than that of seawater (T in Figure 8), to which at larger offsets the refraction arrivals are tangent. Therefore at least some deeper reflections identified in C2 in the MCS data are considered to be reflections from distinctive interfaces; i.e., they are geologically significant.

[39] Apparent velocities of 5.8 ∼ 6.1 km/s for basaltic sills and flows determined from sonobuoys 5 and 6 in C2 are relatively high (Figure 4). The corresponding refraction arrivals occur over a range of source-receiver offsets in which we also observe direct water waves (e.g., 6 in Figure 8), and therefore the apparent velocities are well controlled. As previously mentioned, offset distances were calculated by multiplying observed travel times of direct water waves by a water wave velocity of 1.54 km/s, a reasonable velocity for seawater in the region [e.g., *Abrams et al.*, 1993; *Bruguier and Minshull*, 1997]. However, for the purpose of error estimation, if sound velocity in seawater varies as much as 0.1 km/s, the expected error in velocity would be less than 1%, resulting in an actual velocity of 5.94 km/s for an observed velocity of 6.0 km/s.

[40] An interface interpreted from refraction arrivals on the sonobuoys with velocities of ∼6.0 km/s appears at shallow depths in the transition between the NB and OJP (C3), and further ascends with topography onto the OJP (C4) (Figure 4). Such high velocities are usually not expected at shallow depths, and allows the interpretation that the interface characterizes the top of true oceanic crust in the NB that is continuous to the OJP. However, high velocities have been observed in basalt flows along the Vøring volcanic margin, a large igneous province off central Norway [*Planke and Eldholm*, 1994; *Planke*, 1994]. Individual basalt flows have characteristic velocities of >5 km/s where their thickness exceeds ∼9 m. While the basalt flows along the Vøring margin formed subaerially, those in the Nauru Basin formed in a submarine environment. Due to an absence of subaerial weathering, and proportionally thicker cores of the flows, we would anticipate that the minimum thickness of basalt with velocities as high as ∼6 km/s would be significantly less than the 9 m of those along the Vøring margin (∼9 m). Furthermore, observed thicknesses of basalt sills and flows drilled on the OJP commonly exceed 20 m, reaching a maximum thickness of 65 m [*Fitton et al.*, 2004]. Additionally, sonic logs from DSDP Site 462 showed velocities of 5.5 ∼ 6.0 km/s for basaltic rock samples [*Boyce*, 1981; *Larson and Schlanger*, 1981]. Free-air gravity data aid structural interpretations; a negative gravity anomaly at the transition of the NB and OJP suggests flexure that likely formed by the emplacement of the OJP onto preexisting NB crust (Figure 9), which in simplest terms would require a deeper interface between the base of the OJP and preexisting Late Jurassic-Early Cretaceous oceanic crust. In fact, a model including flexure of the oceanic crust underneath the expected Cretaceous igneous complex at the NB-OJP transition explains the observed gravity anomaly very well. It is reasonable to consider that such high velocities do not necessarily represent properties specific to Late Jurassic-Early Cretaceous oceanic crust.

[41] An evaluation of age-depth models at ODP drill sites in the PB and EMB shows that the plate model (PS [*Parsons and Sclater*, 1977]) has a ∼200 m precision (Table 3, Figure 10). Applying the model to the NB along the Charcot 2 profile running perpendicular to the isochrons, however, results in discrepancies between predicted and observed sediment-corrected values of as much as 1742 m in the center of the basin. We propose that the discrepancies between the predicted and observed depths are explained by the thick igneous complex emplaced during intense Early Cretaceous magmatism in the western Pacific. We estimate a basalt loading factor from a velocity-density relation of basalts sampled at DSDP holes [*Christensen and Salisbury*, 1975]. The factor is ∼890 m/s TWT for

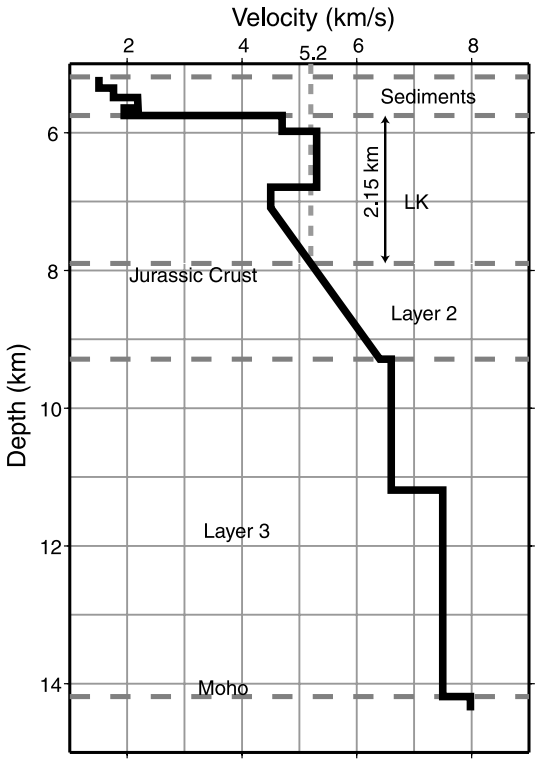

Figure 11. Velocity-depth function at Site 462 in the Nauru Basin (see Figure 3 for location). Layers are interpreted by *Gladczenko et al.* [1997] from previous OBS/sonobuoy wide-angle seismic data [*Houtz*, 1976; *Wipperman et al.*, 1981]. The top of Jurassic oceanic crust may be defined by a P-wave velocity of 5.2 km/s. LK is of the Lower Cretaceous igneous complex with a thickness of 2.15 km.

basalts with a velocity of 4 km/s, and decreases sublinearly with velocity to ~770 m/s TWT for 5.0 km/s basalts. On the basis of existing OBS and sonobuoy data, employing the methodology of *Houtz and Ewing* [1976], *Gladczenko et al.* [1997] proposed that depth to the top of Late Jurassic crust at DSDP Site 462 may be determined by assuming a velocity of 5.2 km/s on the velocity-depth relation. Therefore the thickness of the igneous complex is 2150 m (Figure 11), and its average velocity is ~4.9 km/s, corresponding to a basalt-loading factor of 780 m/s. We apply this factor to differences between predicted and observed sediment-corrected depths to determine thicknesses of the Early Cretaceous igneous complex for the KH98-1 and Charcot 2 seismic data sets; thickness in TWT is translated to thickness in meters by employing an average velocity of 4.9 km/s (Table 2). Our calculations result in a thickness of 2230 m for the igneous complex at Site 462, which agrees with that estimated from seismic data (2150 m) (Figure 11). The complex is thickest, 5464 m, in the center of the basin, and it thins both to the north and south (Figure 5). Our TWT estimates, however, are minima. The factor for basalt loading does not account for the probable existence of sediment between the top of Late Jurassic-Early Cretaceous crust and the Early Cretaceous igneous complex (Figure 5). If such sediment exists, which is likely because of the 14–33 m.y. difference in age between oceanic crust and the igneous complex in the NB (Table 2), an average factor for sediment+basalt loading should be less than the factor for basalts only (780 m/s), which results in a thicker volcanic complex. However, the effect is only significant for thicknesses measured in TWT, because a decrease in the loading factor is commensurate with a decrease in average velocity of the igneous complex and sediment. We have calculated depths to the top of Late Jurassic-Early Cretaceous oceanic crust on the Charcot 2 MCS data at intersections with Lines 201 and 401 using both loading factors (Figure 5).

[42] We observe occasional prominent reflections around and below 8.0 s TWT on the Charcot 2 MCS data (Figure 12). The top of these reflections coincides very well with our calculated depths to the top of Late Jurassic-Early Cretaceous oceanic crust. Without additional data, we cannot be sure that these reflections represent the top of Late Jurassic-Early Cretaceous oceanic crust or the bottom of the Early Cretaceous igneous complex.

[43] Although *Shipley et al.* [1993] interpreted the reflections near 7.0 s TWT to be the top of Late Jurassic-Early Cretaceous oceanic crust on the Charcot 2 profile, we believe that it lies well below the reflections, and that it is more straightforward to identify them as sills/flows for the following reasons:

[44] 1. Refractions with similar velocities of ~6.0 km/s are observed on sonobuoys 5 and 6. However, another refraction interface with a similar velocity lies below the reflections interpreted as the top of the oceanic crust by *Shipley et al.* [1993] (Figures 4 and 6).

[45] 2. Although velocities of ~6.0 km/s seem high for basaltic sills and flows, gravity observations at the transition between the NB and OJP suggest that Late Jurassic-Early Cretaceous oceanic crust lies significantly deeper than the layers characterized by such (see preceding discussion).

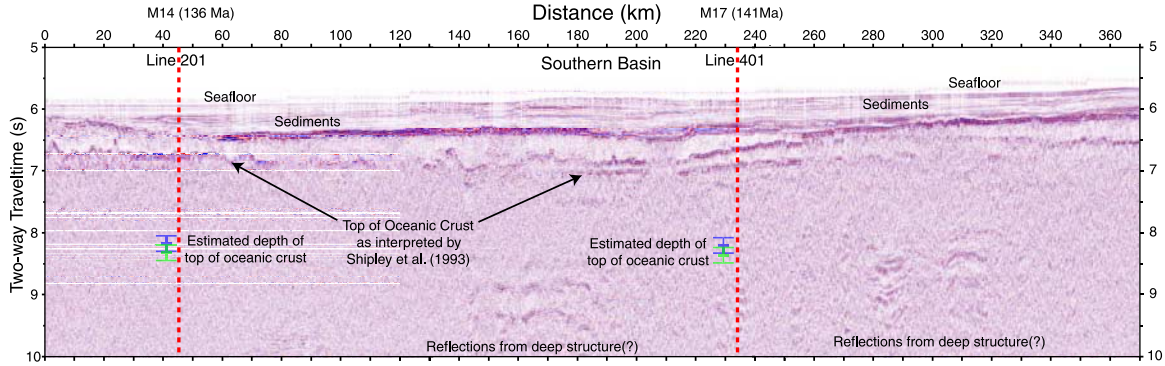

Figure 12. Charcot 2 MCS section (see Figure 3 for location). Estimate depth ranges to the top of oceanic crust at intersections with KH98-1 lines 201 and 401 (red dashed lines) are shown by green (with sediment between the Cretaceous igneous complex and Late Jurassic/Early Cretaceous oceanic crust) and blue (without sediment) bars. A previous interpretation [*Shipley et al.*, 1993] for the top of oceanic crust is indicated by arrows.

[46] 3. The interface interpreted as the top of oceanic crust by *Shipley et al.* [1993] ascends toward a seamount (Figure 7). Unless the seamount is the same age as the oceanic crust, the oceanic crust should descend to form a moat around the seamount [e.g., *Watts and ten Brink*, 1989]. It seems more probable that the interface represents sills or flows.

[47] 4. Our calculated thicknesses of the igneous complex predict that the top of oceanic crust lies at ~8.0 s TWT on the MCS data. We observe prominent reflections at such depths, which suggests that they represent either the bottom of the Early Cretaceous igneous complex or the top of Late Jurassic-Early Cretaceous oceanic crust.

[48] We estimate the volume of the Early Cretaceous igneous complex as follows. We partition the basin into four rectangles (Figure 3), and assume that the thickness of the complex is constant along magnetic isochrons at the northern and southern limits, assigning values of 2230 m and 4288 m, respectively (Table 2). However, the thickness of the complex varies considerably across the central high, and we calculate thicknesses at the rectangles' eastern and western limits individually from water depths in the same manner as along the Charcot 2 profile (4288 m and 4520 m, respectively), while we estimate its thickness at the basin's central high to be 5464 m (Table 2). We assume that the thickness varies linearly along each rectangle's edges between the thickness values given above. The sum of the volumes under the four rectangles is 3.3 million km^3.

[49] Turning to the hypothesis of thermal rejuvenation of oceanic crust, *Nagihara et al.* [1996] estimated the amount of rejuvenation at 14 locations in eight ocean basins of various ages in the western Pacific and the northwest Atlantic. They interpreted that the thermal age of the NB was 50–60 m.y. younger than that indicated by the Mesozoic magnetic anomalies by referring to the sediment thickness and heat flow data from DSDP Site 462. They ascribed the cause of the rejuvenation to massive Early Cretaceous volcanism. However, they only corrected for a sediment thickness of 1.0 s TWT, and did not include corrections for the Cretaceous igneous complex. Our calculations show that the PS predicts depths to Jurassic oceanic crust in the PB and EMB well (Table 3). Ample evidence indicates the widespread distribution of the Early Cretaceous igneous complex in the NB [e.g., *Shipley et al.*, 1993; *Gladczenko et al.*, 1997; *Castillo*, 2004], and the loading effect of its ~3.3 million km^3 volume must be taken into consideration.

8. Conclusions

[50] Our MCS/refraction data set consists of two profiles; one profile extends from the center of the Nauru Basin to the eastern flank of the Ontong Java Plateau, and the other lies in the southernmost Nauru Basin just north of the OJP's eastern salient. Acoustic basement structure along the transect in the Nauru Basin may be divided into three major sections: C1, reflection-free basement resulting from Early Cretaceous volcanic activity; C2, dipping sills and flows; and C3, massive volcanic activity related to emplacement of the OJP. Another segment, C4, encompasses the OJP.

[51] Basaltic sills and flows in the basin have relatively high velocities of ~6.0 km/s. However, we observe traces of sills and flows on the MCS

sections only in a limited area of the southern basin ~90 km across. The dominant acoustic basement structure in the basin consists of a thick, relatively reflection-free volcanic complex, from which refraction arrivals are observed only rarely.

[52] The plate model proposed by *Parsons and Sclater* [1977] predicts depths to oceanic crust, corrected for sediment loading [*Crough*, 1983], well at three drill sites in the Pigafetta and East Mariana Basins. When the model is applied to the Nauru Basin, where the seafloor is ~1000 m shallower than in the other two ocean basins, large discrepancies exist between predicted and observed depths. However, these discrepancies may be explained by the Early Cretaceous igneous complex, with a maximum thickness of 5500 m in the center of the basin where the depth to the seafloor is shallowest. The bathymetry of the Nauru Basin likely reflects the thickness of the complex.

[53] We believe that the interface that has been interpreted as the top of Late Jurassic-Early Cretaceous oceanic crust by *Shipley et al.* [1993] probably corresponds to sills or flows, and that the top of the crust actually lies deeper, perhaps ~2.0 s TWT below the seafloor. We estimate the total volume of the Early Cretaceous igneous complex to be 3.3 million km^3.

[54] The Nauru Basin remains enigmatic in considering preservation of Late Jurassic-Early Cretaceous magnetic anomalies below such an Early Cretaceous igneous complex. Further basin-wide crustal studies are needed to provide a more comprehensive understanding.

Acknowledgments

[55] The authors thank the captain and crew of R/V *Hakuho Maru* of the Ocean Research Institute, University of Tokyo, for their skillful deployment and retrieval of equipment. Technical support from M. Wiederspahn was essential for the success of the survey. Special thanks are due to Y. Aoyagi, E. Araki, T. Gladczenko, C. Igarashi, G. Ito, L. Kroenke, R. Larson, S. Miura, M. Nishino, T. Sato, M. Shinohara, and S. Yoneshima for their assistance during cruise KH98-1. We are grateful to include MCS data from the Charcot87 cruise (PI: Y. Lancelot), retrieved from the Web site of Marine Geosciences Seismic Data Management System, Institute for Geophysics, University of Texas at Austin. We also thank Editor W. White, Associate Editor J. Dixon, and two anonymous reviewers for their careful reviews that improved the manuscript. M.F.C. was supported by grants from the U.S. National Science Foundation (OCE-9714368 and INT-9903454), Joint Oceanographic Institutions/U.S. Science Support Program, and the Japanese Ministry of Education, Culture, Sports, Science, and Technology (MEXT). This study forms part of the collaborative Japan-U.S. programs in the Western Pacific.

References

Abrams, L. J., R. L. Larson, T. H. Shipley, and Y. Lancelot (1993), Cretaceous volcanic sequences and Jurassic oceanic crust in the East Mariana and Pigafetta Basins of the western Pacific, in *Mesozoic Pacific*, *Geophys. Monogr. Ser.*, vol. 77, edited by M. Pringle et al., pp. 103–119, AGU, Washington, D. C.

Bercovici, D., and J. Mahoney (1994), Double flood basalts and plume head separation at the 660-kilometer discontinuity, *Science*, *266*, 1367–1369.

Boyce, E. R. (1981), Electrical resistivity, sound velocity, thermal conductivity, density-porosity, and temperature, obtained by laboratory techniques and well logs: Site 462 in the Nauru Basin of the Pacific Ocean, *Initial Rep. Deep Sea Drill. Proj.*, *61*, 743–761.

Bruguier, N. J., and T. A. Minshull (1997), Accurate modelling of sonobuoy refraction data to determine velocity variations in oceanic crust, *Mar. Geophys. Res.*, *19*, 25–36.

Cande, S. C., R. L. Larson, and J. L. LaBrecque (1978), Magnetic lineations in the Pacific Jurassic Quiet Zone, *Earth Planet. Sci. Lett.*, *41*, 434–440.

Castillo, P. R. (2004), Geochemistry of Cretaceous volcaniclastic sediments in the Nauru and East Mariana Basins provides insights into the mantle sources of giant oceanic plateaus, in *Origin and Evolution of the Ontong Java Plateau*, edited by J. G. Fitton et al., *Geol. Soc. Spec. Publ.*, *229*, 353–368.

Castillo, P. R., R. W. Carlson, and R. Batiza (1991), Origin of Nauru Basin igneous complex: Sr, Nd and Pb isotope and REE constraints, *Earth Planet. Sci. Lett.*, *103*, 200–213.

Castillo, P. R., M. S. Pringle, and R. W. Carlson (1994), East Mariana Basin tholeiites: Cretaceous intraplate basalts or rift basalts related to the Ontong Java plume?, *Earth Planet. Sci. Lett.*, *123*, 139–154.

Christensen, N. I., and M. H. Salisbury (1975), Structure and constitution of the lower oceanic crust, *Rev. Geophys.*, *13*, 57–86.

Coffin, M. F., and O. Eldholm (1993), Scratching the surface: Estimating dimensions of large igneous provinces, *Geology*, *21*, 515–518.

Crough, T. S. (1983), The correction for sediment loading on the seafloor, *J. Geophys. Res.*, *88*, 6449–6454.

Farnetani, C. G., and M. A. Richards (1994), Numerical investigations of the mantle plume initiation model for flood basalts, *J. Geophys. Res.*, *99*, 13,813–13,833.

Fitton, J. G., and M. Godard (2004), Origin and evolution of magmas on the Ontong Java Plateau, in *Origin and Evolution of the Ontong Java Plateau*, edited by J. G. Fitton et al., *Geol. Soc. Spec. Publ.*, *229*, 151–178.

Fitton, J. G., J. J. Mahoney, P. J. Wallace, and A. D. Saunders (2004), Leg 192 synthesis: Origin and evoluction of the Ontong Java Plateau, in *Proc. Ocean Drill. Program Sci. Results*, *192*, 1–18.

Gladczenko, T. P., M. F. Coffin, and O. Eldholm (1997), Crustal structure of the Ontong Java Plateau: Modeling of new gravity and existing seismic data, *J. Geophys. Res.*, *102*, 22,711–22,729.

Gradstein, F. M., F. P. Agterberg, J. G. Ogg, J. Hardenbol, P. van Veen, J. Thierry, and Z. Huang (1994), A Mesozoic time scale, *J. Geophys. Res.*, *99*, 24,051–24,074.

Hamilton, E. (1978), Sound velocity-density relations in sea-floor sediments and rocks, *J. Acoust. Soc. Am.*, *63*, 366–377.

Houtz, R. E. (1976), Seismic properties of Layer 2A in the Pacific, *J. Geophys. Res.*, *81*, 6321–6331.

Houtz, R., and J. Ewing (1976), Upper crustal structure as a function of plate age, *J. Geophys. Res.*, *81*, 2490–2498.

Ingle, S., and M. F. Coffin (2004), Impact origin for the greater Ontong Java Plateau?, *Earth Planet. Sci. Lett.*, *218*, 123–134.

Larson, R. L. (1976), Late Jurassic and Early Cretaceous evolution of the western central Pacific Ocean, *J. Geomagn. Geoelectr.*, *28*, 219–236.

Larson, R. L. (1991), Latest pulse of Earth: Evidence for a mid Cretaceous superplume, *Geology*, *19*, 547–550.

Larson, R. L., and S. O. Schlanger (1981), Geological evolution of the Nauru Basin, and regional implications, in *Initial Rep. Deep Sea Drill. Proj.*, *61*, 841–862.

Nagihara, S., C. R. B. Lister, and J. G. Sclater (1996), Reheating of old oceanic lithosphere: Deductions from observations, *Earth Planet. Sci. Lett.*, *139*, 91–104.

Nakanishi, M., and E. L. Winterer (1998), Tectonic history of the Pacific-Farallon-Phoenix triple junction from Late Jurassic to Earth Cretaceous: An abandoned Mesozoic spreading system in the Central Pacific Basin, *J. Geophys. Res.*, *103*, 12,453–12,468.

Nakanishi, M., K. Tamaki, and K. Kobayashi (1992), A new Mesozoic isochron chart of the northwestern Pacific Ocean: Paleomagnetic and tectonic implications, *Geophys. Res. Lett.*, *19*, 693–696.

Ozima, M., K. Saito, and Y. Takigami (1981), $^{40}Ar/^{39}Ar$ geochronological studies on rocks drilled at Holes 462 and 462A, Deep Sea Drilling Project Leg 61, *Initial Rep. Deep Sea Drill. Proj.*, *61*, 841–862.

Parsons, B., and J. G. Sclater (1977), An analysis of the variation of ocean floor bathymetry and heat flow with age, *J. Geophys. Res.*, *82*, 803–827.

Planke, S. (1994), Geophysical response of flood basalts from analysis of wire line logs: Ocean Drilling Program Site 642, Vøring volcanic margin, *J. Geophys. Res.*, *99*, 9279–9296.

Planke, S., and O. Eldholm (1994), Seismic response and construction of seaward dipping wedges of flood basalts: Vøring volcanic margin, *J. Geophys. Res.*, *99*, 9263–9278.

Renkin, M., and J. G. Sclater (1988), Depth and age in the North Pacific, *J. Geophys. Res.*, *93*, 2919–2935.

Rogers, G. C. (1982), Oceanic plateaus as meteorite impact signatures, *Nature*, *299*, 341–342.

Shipboard Scientific Party (1986), Site 462, *Initial Rep. Deep Sea Drill. Proj.*, *89*, 157–211.

Shipley, T. H., L. J. Abrams, Y. Lancelot, and R. L. Larson (1993), Late Jurassic-Early Cretaceous oceanic crust and Early Cretaceous volcanic sequences of the Nauru Basin, western Pacific, in *Mesozoic Pacific*, *Geophys. Monogr. Ser.*, vol. 77, edited by M. Pringle et al., pp. 77–101, AGU, Washington, D. C.

Stein, C., and S. Stein (1992), A model for the global variation in oceanic depth and heat flow with lithospheric age, *Nature*, *359*, 123–129.

Takigami, Y., S. Amari, M. Ozima, and R. Moberly (1986), $^{40}Ar/^{39}Ar$ geochronological studies of basalts from Hole 462A, Nauru Basin, Deep Sea Drilling, Project Leg 89, *Initial Rep. Deep Sea Drill. Proj.*, *89*, 519–521.

Talwani, M., J. L. Worzel, and M. Landisman (1959), Rapid gravity computations for two-dimensional bodies with application to the Mendocino submarine fracture zone, *J. Geophys. Res.*, *64*, 45–59.

Tarduno, J. A., W. V. Sliter, L. Kroenke, M. Leckie, H. Mayer, J. J. Mahoney, R. Musgrave, M. Storey, and E. L. Winterer (1991), Rapid formation of Ontong Java Plateau by Aptian mantle plume volcanism, *Science*, *25*, 399–403.

Tejada, M. L. G., J. J. Mahoney, P. R. Castillo, S. P. Ingle, H. C. Sheth, and D. Weis (2004), Pin-pricking the elephant: Evidence on the origin of the Ontong Java Plateau from Pb-Sr-Hf-Nd isotopic characteristics of ODP Leg 192 basalts, in *Origin and Evolution of the Ontong Java Plateau*, edited by J. G. Fitton et al., *Geol. Soc. Spec. Publ. 229*, 133–150.

Watts, A. B., and U. S. ten Brink (1989), Crustal structure, flexure and subsidence history of the Hawaiian Islands, *J. Geophys. Res.*, *94*, 10,473–10,500.

Wipperman, L. K., R. L. Larson, and D. M. Hussong (1981), The geological and geophysical setting near Site 462, *Initial Rep. Deep Sea Drill. Proj.*, *61*, 841–862.